Long-term and seasonal trends in stratification in the California Current, 1950–1993

Daniel M. Palacios, Steven J. Bograd, Roy Mendelssohn, and Franklin B. Schwing
Pacific Fisheries Environmental Laboratory, National Marine Fisheries Service, NOAA, Pacific Grove, California, USA

Received 11 March 2004; revised 15 July 2004; accepted 4 August 2004; published 30 October 2004.

[1] State-space model decomposition of subsurface temperatures from the World Ocean Database is used to detect and characterize changes in thermal stratification in the upper 200 m of the California Current System (CCS) over the period 1950–1993. Model results are analyzed at eight locations representing the meridional and offshore extent of the CCS between 31°N and 40°N. Thermocline strength, depth, and temperature are derived from the mean-level trend term and the seasonal component of the state-space models. Over the 44 years, the mean level of the coastal thermocline strengthened and deepened, while it weakened and shoaled offshore. These tendencies are likely the result of geostrophic adjustment to changes in basin-scale circulation, as well as to a long-term increase in upper ocean heat content of 2–9% throughout the study area. Reduction in nutrient inputs to the surface layer resulting from these climate signals are a likely explanation for the pronounced decline in biological production in CCS ecosystems observed over the same period. Substantial decadal variability superimposed on these linear tendencies may play a role in determining the response of the upper ocean to interannual events such as El Niño. The seasonal component of thermocline depth and strength exhibited a high degree of nonstationarity, with alternating periods of weakened and enhanced annual cycles lasting 3–5 years, along with changes in the phase. This changing seasonality may have implications for marine species whose life cycles are closely tuned to the seasonal cycle. *INDEX TERMS:* 4215 Oceanography: General: Climate and interannual variability (3309); 4516 Oceanography: Physical: Eastern boundary currents; 4522 Oceanography: Physical: El Nino; 4572 Oceanography: Physical: Upper ocean processes; *KEYWORDS:* thermal stratification, trends, nonstationary seasonality, California Current

Citation: Palacios, D. M., S. J. Bograd, R. Mendelssohn, and F. B. Schwing (2004), Long-term and seasonal trends in stratification in the California Current, 1950–1993, *J. Geophys. Res.*, *109*, C10016, doi:10.1029/2004JC002380.

1. Introduction

[2] High biological production in coastal upwelling ecosystems such as the California Current System (CCS) is fueled by the introduction of nutrients from the deep ocean in response to wind-forcing. The strength and depth of the maximum stratification in the water column regulate the entrainment of nutrients from below the thermocline, such that an anomalously deep, strong thermocline, if persistent over long periods, can result in long-term reductions in biological production and in ecosystem changes. Indeed, long-term fluctuations in biological production within the CCS have been associated with climatic variability on interannual to decadal scales [*Chelton et al.*, 1982; *Roemmich and McGowan*, 1995; *McGowan et al.*, 2003].

[3] Climate forcing can also have a large impact on important seasonal processes. For example, long-term changes in the phase and amplitude of coastal upwelling [*Schwing and Mendelssohn*, 1997, 1998] and of the "spring transition" from winter to upwelling conditions [*Lynn et al.*, 2003] have been described in the CCS. Since many marine species have life cycles closely tuned to the seasonal cycle, a changing seasonality can lead to mismatches in characteristic trophic interactions [*Cushing*, 1969, 1975] and variations in ecosystem structure and productivity [*Broekhuizen and McKenzie*, 1995; *Beare et al.*, 1998; *Beare and McKenzie*, 1999; *Bograd et al.*, 2002].

[4] Two recent papers [*Mendelssohn et al.*, 2003, 2004] used state-space models to examine the long-term trends and seasonal behavior of subsurface temperatures in the upper 200 m at a number of locations within the CCS over the period 1950–1993. Both studies revealed different trends within the mixed layer and underlying thermocline, implying significant variability in thermal stratification. Variability in upper ocean stratification regulates nutrient availability in the euphotic zone and affects biological production and community composition [e.g., *Le Quéré et al.*, 2003; *Field*, 2004]. In this paper, we extend the analyses of *Mendelssohn et al.* [2003, 2004] to examine long-term and seasonal changes in the depth of the thermocline, the strength of stratification, and upper ocean heat content

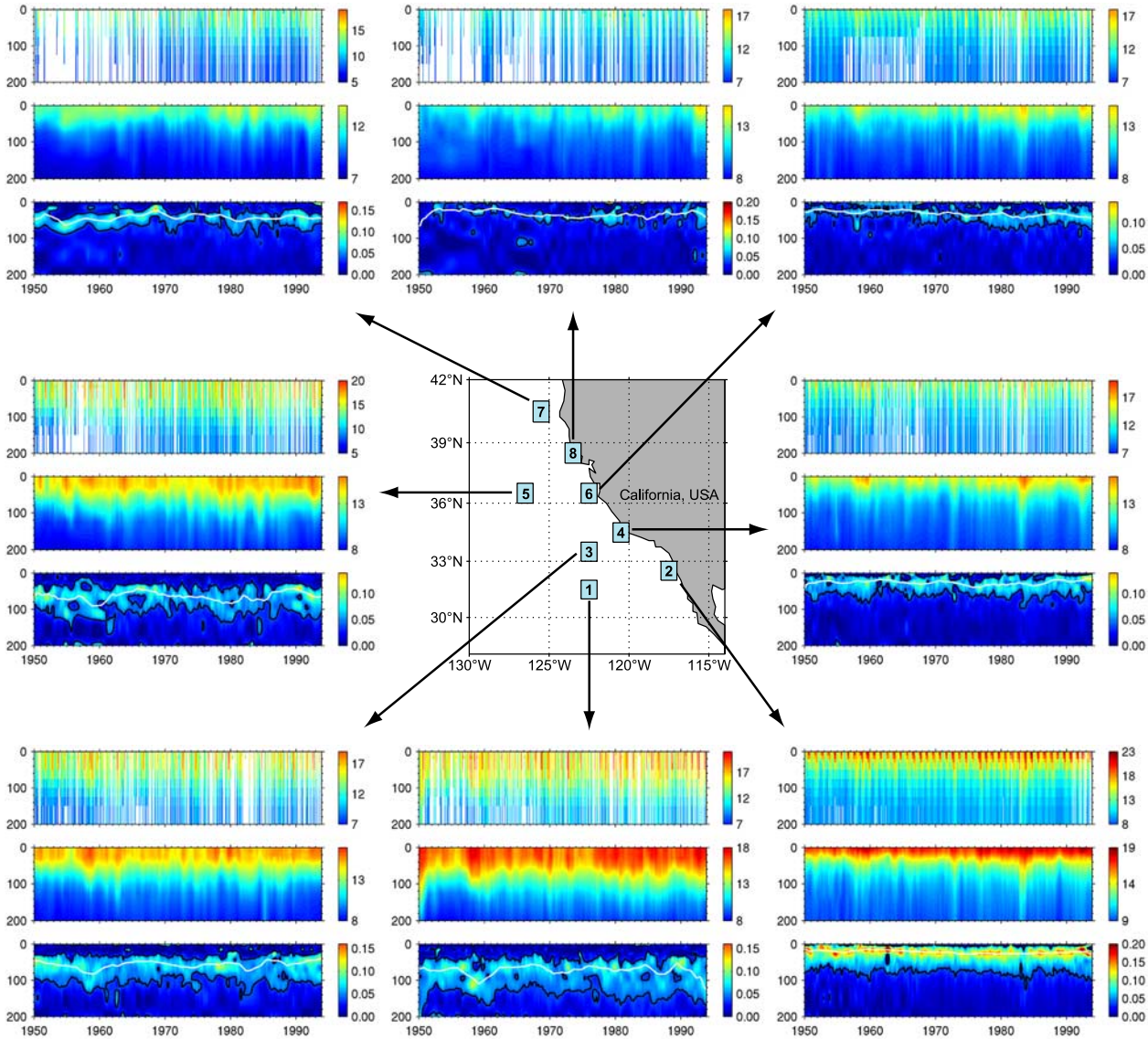

Figure 1. Water column monthly time series at eight locations in the CCS, 1950–1993. At each location, the (top panel) observed 0–200 m temperature (°C), (middle panel) modeled long-term trend component (°C), and (bottom panel) dT/dz (°C m^{-1}) are shown. The black curve in each of the bottom panels corresponds to the 0.04°C m^{-1} contour, and the white curve is the depth of maximum dT/dz (m) (smoothed with a 37-point running average).

within the CCS over the same period. These results are interpreted within the context of observed long-term changes in biological production in the region.

2. Materials and Methods

2.1. Data Series

[5] Upper ocean temperature observations at 10 standard depth levels (0, 10, 20, 30, 50, 75, 100, 125, 150, and 200 m) for the period 1950–1993 were obtained from the World Ocean Database 1998 [*Conkright et al.*, 1999], and binned into monthly series at one-degree resolution. Owing to the relative sparsity of salinity data, this study is restricted to an area in the CCS between 31°N and 40°N where stratification is mainly driven by temperature [e.g., *Kara et al.*, 2003]. Eight locations with ample data representing the meridional and offshore extent of the CCS within this area were selected for detailed study (Figure 1). Four locations are considered "coastal" in character (2, 4, 6, and 8) and four are considered "offshore" (1, 3, 5, and 7) (Table 1). Blatant outliers were removed from each series, and state-space models were then applied to these data, as described in the next section.

2.2. State-Space Modeling

[6] State-space models, as implemented for oceanographic time series [e.g., *Schwing and Mendelssohn*, 1997; *Durand and Mendelssohn*, 1998], were used to decompose the data into a mean-level "trend term" (nonstationary and nondeterministic), a "seasonal component" (zero-

Table 1. Geographic Coordinates, Character, and Number of Observations at the Eight Locations Used in the Study[a]

Location	Coordinates	Character	Number of Observations
1	31°N, 123°W	offshore	334
2	32°N, 118°W	coastal	514
3	33°N, 123°W	offshore	337
4	34°N, 121°W	coastal	389
5	36°N, 127°W	offshore	378
6	36°N, 123°W	coastal	479
7	40°N, 126°W	offshore	253
8	38°N, 124°W	coastal	274

[a]For months with at least one observation at one depth, for the period 1950–1993 (528 months). Location coordinates refer to the southwest corner of the 1° boxes.

mean, nonstationary, and nondeterministic), an ''irregular term'' (containing any stationary autocorrelated part of the data), and a measurement ''error term'' (zero-mean, stationary, and uncorrelated). This decomposition was applied to each individual time series independently (i.e., by fitting a univariate model at each one of the 10 depth levels and eight locations, for a total of 80 time series).

[7] The terms in the state-space model decomposition are constrained by piecewise continuous smoothing splines and are solved by using a combination of the Kalman filter and maximum likelihood estimation (see *Durand and Mendelssohn* [1998] for details). The method produces statistically consistent estimates of the components, and has the ability to interpolate over data gaps. These estimates, however, have a greater potential for bias during periods with large data gaps (e.g., the earlier part of the record at locations 7 and 8, Figure 1) than periods with more uniform coverage. Therefore we place most emphasis on periods with reasonable data coverage.

[8] In two recent papers, *Mendelssohn et al.* [2003, 2004] used the trend term and the seasonal component of a larger set of the series used in this study to identify the dominant patterns of spatial and temporal variability in subsurface temperatures throughout the CCS. Here we focus on the particular region of the water column where maximum stratification occurs.

2.3. Variables Derived

[9] Water column stratification was studied for both the nonseasonal trend term and the seasonal component of the subsurface temperatures yielded by the state-space models. As an initial step, smoothly varying profiles at 1-m resolution were obtained for both components by cubic spline interpolation of each monthly profile at the discrete standard depths. For the trend term, the vertical temperature gradient dT/dz was computed from these data as a measure of stratification. Graphical inspection of the dT/dz time series indicated that the strongest gradient (i.e., the thermocline) was contained within the depth range generally bounded by the 0.04°C m^{-1} contour (see bottom panels in Figure 1). Thus, at each time step, the maximum value of dT/dz, the depth of that maximum, and the temperature at that maximum within this depth range were extracted as indicators of the strength, depth, and temperature of the thermocline, respectively. The thermocline depth will generally be distinct from (deeper than) the turbulent mixed layer depth, which has a dT/dz near zero (see Figure 1). Only in the nearshore location in the Southern California Bight (location 2), where the thermocline is very shallow, might these two depths be comparable. For times when dT/dz values throughout the water column were less than 0.04°C m^{-1} (e.g., locations 6–8 in Figure 1), the variables of interest were extracted from within a depth range computed from the averaged depth of the 0.04°C m^{-1} bounds at the times when dT/dz reached that value at that particular location. Outliers in the resulting time series were eliminated with three iterations of a median filter, such that for a given sliding window, values outside 3 standard deviations were replaced with the median value of the window. Window sizes were three, five, and three points. Finally, the series were smoothed with a 37-point running average filter to emphasize low-frequency (i.e., greater than ENSO) variability in the assessment of long-term trends described in the next section.

[10] The seasonal component in the state-space model is a zero-mean term that varies around the time-dependent mean (i.e., the trend term). To derive the seasonal contribution to the strength and depth of the thermocline, the 1-m resolution seasonal component temperatures were added to the 1-m resolution trend-term temperatures. The vertical gradient was then computed for these ''mean level plus seasonal deviations'' temperatures, and the values for maximum dT/dz and depth of maximum dT/dz were extracted from the region in the water column containing the maximum gradient, as was done for the trend term. These series were then despiked with a recursive 3-5-3 median filter. Finally, variations in strength and depth of the thermocline due solely to the seasonal cycle were obtained by subtracting the smoothed trend-term series, above, from the despiked ''mean level plus seasonal deviations'' series just described.

[11] To gain additional understanding of the thermal variability in the CCS during the study period, vertically integrated heat content (HC) was computed for the trend-term temperatures by integrating over the 0–200 m range using the formula: $HC = c_p\bar{\rho} \int T(z)dz$, where the specific heat of seawater c_p = 3990 J kg^{-1} °C^{-1} and the mean density of seawater $\bar{\rho}$ = 1025 kg m^{-3}. These series were also smoothed with a 37-point running average to emphasize low-frequency variability. Additionally, heat content was computed from the surface to the depth of the thermocline, and this integration was subtracted from the unsmoothed version of the 0–200 m integration. The difference between the two integrations was used for determining the thermal impact of different El Niño (EN) events in the thermocline of the CCS, as described in the next section.

2.4. Assessment of Trends

[12] A series-long, area-wide warming tendency was reported by *Mendelssohn et al.* [2003] in their study of subsurface temperatures. To assess whether a secular trend was present in the thermocline variables derived in this study, simple linear regression was applied to the smoothed trend-term series. *Mendelssohn et al.* [2003] also observed a variable response in the depth distribution of the temperature signals associated with different EN events, with some events featuring a much stronger near-surface signal, while others appeared to be more concentrated in the thermocline.

Table 2. Estimates for the Slope Parameter (±95% Confidence Interval), the Coefficient of Determination, and the p Statistic for the Regression of the Smoothed Time Series of Maximum dT/dz, Depth of Maximum dT/dz, and Temperature at the Depth of Maximum dT/dz on Year at Eight Locations in the CCS for the Period 1950–1993[a]

	Maximum dT/dz				
Location	Mean, °C m^{-1}	Slope, °C m^{-1} (44 yr)$^{-1}$	Percent Change	R^2, %	p-Value
1	0.075	−0.0008 ± 0.0025	−1.1	0.1	0.5197
2	0.135	−0.0079 ± 0.0047	−5.7	2.1	0.0009
3	0.076	0.0013 ± 0.0036	1.7	0.1	0.4877
4	0.077	0.0207 ± 0.0028	31.2	28.7	<0.0001
5	0.075	−0.0056 ± 0.0038	−7.1	1.6	0.0041
6	0.060	0.0217 ± 0.0017	44.2	54.1	<0.0001
7	0.068	−0.0180 ± 0.0028	−23.2	23.0	<0.0001
8	0.048	0.0126 ± 0.0025	30.2	16.0	<0.0001
	Z(Maximum dT/dz)				
Location	Mean, m	Slope, m (44 yr)$^{-1}$	Percent Change	R^2, %	p-Value
1	72.7	−0.38 ± 3.67	0.5	0.01	0.8376
2	21.9	−8.71 ± 0.80	49.6	46.4	<0.0001
3	56.7	10.39 ± 2.59	−16.8	10.6	<0.0001
4	26.3	−1.08 ± 1.63	4.2	0.3	0.1936
5	64.2	6.65 ± 3.42	−9.9	2.7	0.0001
6	31.0	−17.93 ± 1.21	81.5	61.8	<0.0001
7	42.5	4.70 ± 2.24	−10.5	3.1	<0.0001
8	32.7	−9.79 ± 2.37	35.2	11.1	<0.0001
	Temperature at Z(Maximum dT/dz)				
Location	Mean, °C	Slope, °C (44 yr)$^{-1}$	Change, °C	R^2, %	p-Value
1	13.9	0.78 ± 0.19	0.78	10.6	<0.0001
2	15.5	0.75 ± 0.13	0.75	21.0	<0.0001
3	13.2	0.88 ± 0.12	0.88	27.4	<0.0001
4	12.9	1.27 ± 0.14	1.26	36.1	<0.0001
5	12.7	1.33 ± 0.14	1.33	38.4	<0.0001
6	12.0	0.78 ± 0.10	0.78	29.0	<0.0001
7	11.4	0.61 ± 0.09	0.61	25.1	<0.0001
8	11.2	1.01 ± 0.12	1.01	35.6	<0.0001

[a]Also reported are the series mean and the percent change in the series corresponding to the computed linear trend. For temperature, the absolute change, rather than the percent change, is given.

The heat content between the thermocline and 200 m (i.e., the difference between the two integrations) was used as an indicator of the relative distribution of heat anomalies in the water column during strong EN events. Changes in the amplitude and phase of the seasonal cycle were determined from the derived maximum dT/dz and depth of maximum dT/dz seasonal series.

3. Results

3.1. Mean Stratification Patterns and Long-Term Trends

[13] The depth range bounded by the 0.04°C m^{-1} contour in the temperature gradient dT/dz (bottom panels in Figure 1) gives an indication of the location of the thermocline in the water column. In general, the thermocline is thick in the south and thins out to the north. Pronounced cross-shore and alongshore patterns are also evident in the maximum dT/dz (i.e., the strength of the thermocline) and in the depth of that maximum (i.e., the depth of the thermocline). Time-averaged values show that at the coastal locations the thermocline is strong to the south (0.14°C m^{-1}) and weakens progressively toward the north (0.05°C m^{-1}), while offshore the strength of the thermocline persists at intermediate values across all locations (0.07°–0.08°C m^{-1}) (Table 2). The time-averaged values of depth of the thermocline (Table 2) show that it is shallow at the coast (22–33 m) and deep offshore (43–73 m). This cross-shore pattern is further contrasted by a coastal deepening and a pronounced offshore shoaling from south to north. Average temperatures in the thermocline decrease from south to north at all locations (15.5°–11.2°C) (Table 2), concomitant with a latitudinal decrease in water column heat content (10.3–7.9 × 10^9 J m^{-2}) (Table 3). On average, the coastal thermocline tends to be cooler (except for location 2 in the Southern California Bight) and has lower heat content than the offshore thermocline.

[14] Simple linear regression indicates that statistically significant increases in strength of the thermocline of 0.013°–0.022°C m^{-1} over the 44-year period have occurred at coastal locations 4, 6, and 8, while decreases of 0.006°–0.018°C m^{-1} have occurred at offshore locations 5 and 7 (Table 2, Figure 2). The thermocline has significantly deepened by 9–18 m at coastal locations 2, 6, and 8, while shoaling of 5–10 m has occurred at offshore locations 3, 5, and 7 (Table 2, Figure 2). Thermocline behavior in the Southern California Bight (location 2) was unique in that it weakened by 0.008°C m^{-1} while at the same time it deepened by almost 9 m over the study period. Significant increases in thermocline temperatures have occurred at all locations, ranging from 0.6°C to 1.3°C over the 44-year period (Table 2, Figure 2). Likewise, 0–200 m heat content has increased at all locations by ~2–8 × 10^8 J m^{-2}, or about 2–9% (Table 3, Figure 3).

Table 3. Estimates for the Slope Parameter (±95% Confidence Interval), the Coefficient of Determination, and the *p* Statistic for the Regression of the Smoothed Time Series of 0–200 m Heat Content on Year at Eight Locations in the CCS for the Period 1950–1993[a]

Location	Mean ($\times 10^9$ J m^{-2})	Slope ($\times 10^8$ J m^{-2} (44 yr)$^{-1}$)	Percent Change	R^2, %	*p*-Value
1	10.3	5.4 ± 0.9	5.4	20.0	<0.0001
2	9.5	8.2 ± 0.6	9.1	58.7	<0.0001
3	9.3	2.2 ± 0.5	2.4	11.0	<0.0001
4	8.7	7.1 ± 0.6	8.5	50.2	<0.0001
5	9.3	6.3 ± 0.5	7.1	49.4	<0.0001
6	8.3	5.9 ± 0.6	7.4	46.0	<0.0001
7	7.9	4.1 ± 0.6	5.4	26.4	<0.0001
8	8.0	4.8 ± 0.5	6.2	40.4	<0.0001

[a]Also reported are the series mean and the percent change in the series corresponding to the computed linear trend.

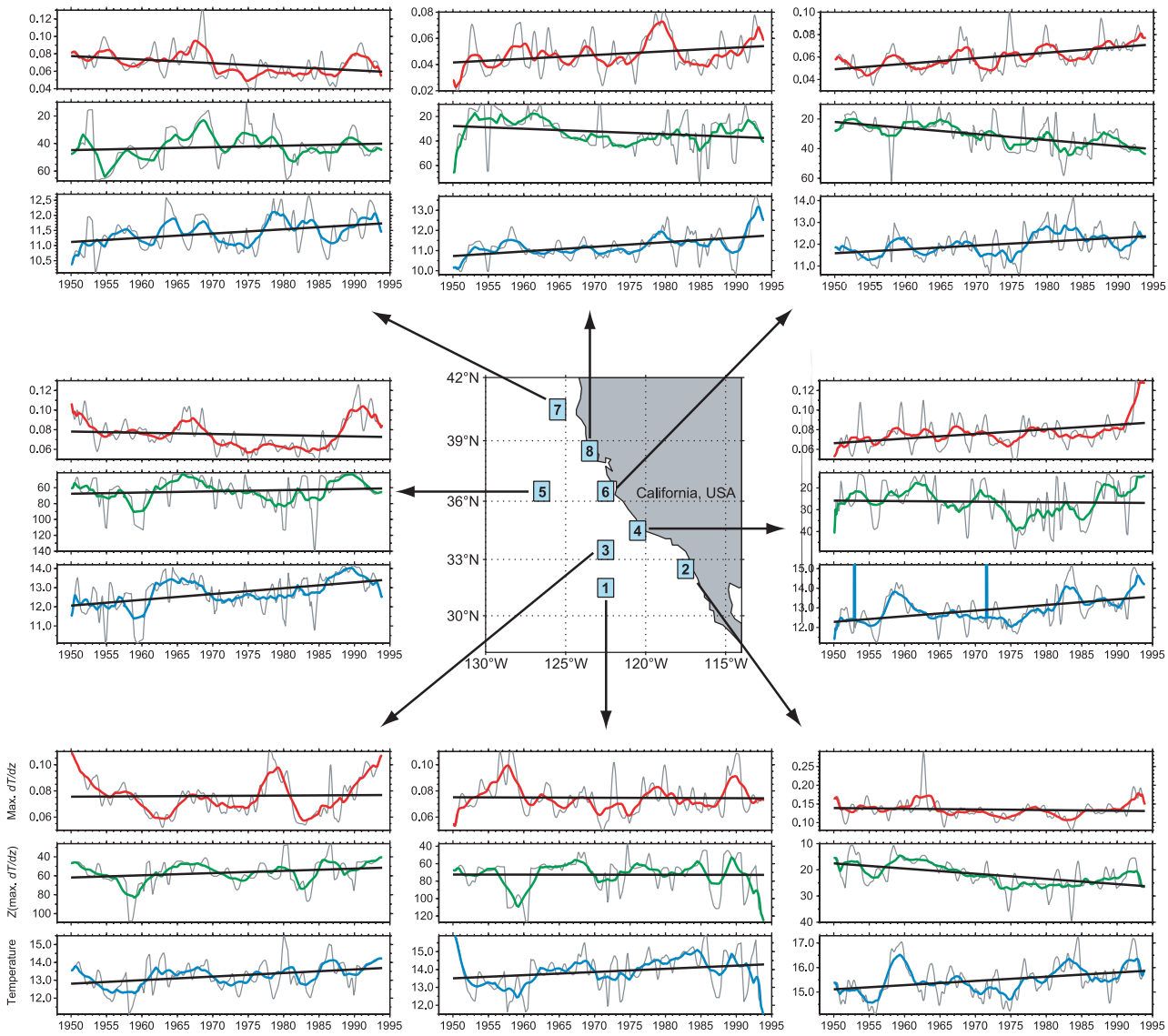

Figure 2. Time series of variables derived from the modeled trend component at eight locations in the CCS, 1950–1993. At each location, the (top panel) maximum dT/dz (°C m^{-1}), (middle panel) depth of the maximum dT/dz (m), and (bottom panel) temperature at the depth of the maximum dT/dz (°C) are shown. Light gray curves are the monthly series, and colored curves are the 37-point running averages. The regression of each variable on year is indicated by the black line.

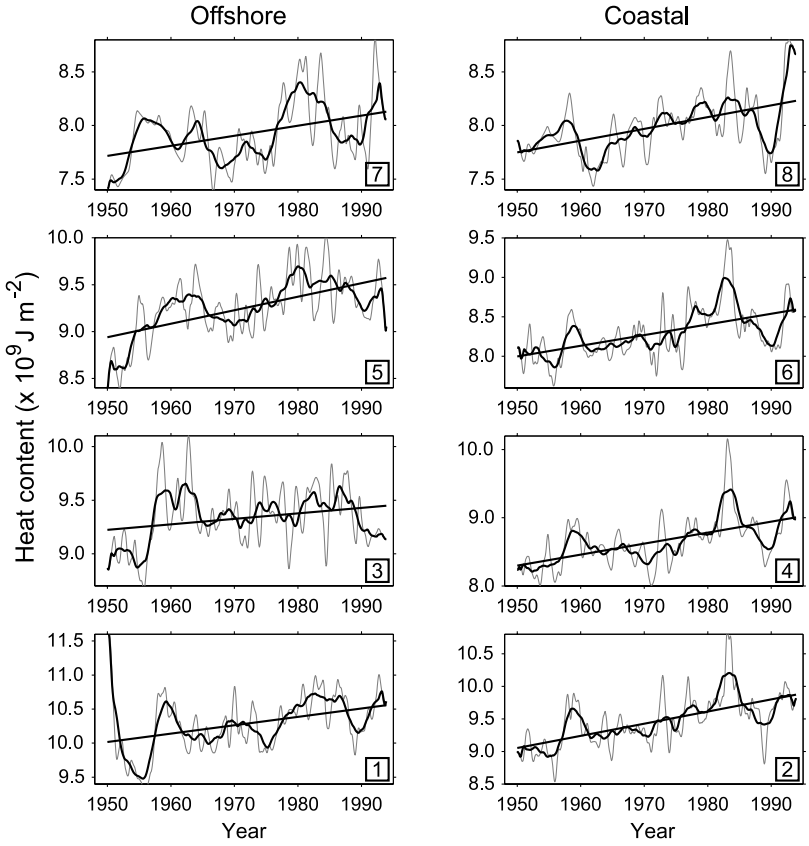

Figure 3. Time series of 0–200 m heat content ($\times 10^9$ J m^{-2}) derived from the modeled trend component at eight locations in the CCS, 1950–1993. Light gray curves are the monthly series, and black curves are the 37-point running averages. The regression of heat content on year is indicated by the black line. Locations are identified by numbered boxes.

[15] Variability in temperatures associated with the depth of maximum stratification (Figure 2) suggests that the common practice of using the depth of a particular isotherm (e.g., 12°C) as an indicator of the depth of the thermocline may not be the most appropriate approach in long-term studies. This is particularly true if the thermal structure of the area of maximum stratification changes such that the chosen isotherm is not contained in it.

3.2. El Niño Variability

[16] The effects of EN on the thermocline variables can be readily seen in the unsmoothed version of the trend-term time series (light gray curves in Figure 2). These are examined in more detail for coastal location 6, and contrasted with location 5, directly offshore (Figure 4). Highlighted in these plots are the strong tropical EN events of 1957–1958, 1972–1973, 1982–1983, and 1986–1987. Marked spikes coincident with these periods are evident at the coastal location in all the series, while the effect is nearly indiscernible from other short-term (i.e., interannual) variations at the offshore location (Figure 4). This lack of a clear offshore signal is expected, as the thermocline is located significantly deeper at the offshore location (64.2 m) than it is at the coastal one (31 m). Indeed, the principal means by which the EN signal is imparted to the CCS is by surface Ekman processes and oceanic teleconnections, neither of which will have a strong impact on the offshore thermocline.

[17] Different EN events were associated with clearly different responses in coastal CCS water column structure. For instance, the large heat content difference between the two integration depths during the 1972–1973, 1982–1983, and 1986–1987 events indicates that these were "deep events" (i.e., maximum warming occurred below the thermocline) (Figure 4h). In contrast, the 1957–1958 event was a "shallow event" affecting primarily the waters above the thermocline, as indicated by the small heat content difference between the two layers (Figure 4h).

[18] These differences are consistent with the analysis of *Mendelssohn et al.* [2003], who classified warm and cool events in the CCS based on the geographical and depth-dependent characteristics of their temperature signatures. The thermocline depth reveals a shallow period between 1950 and 1966 (when the 1957–1958 event took place) followed by a deep period between 1969 and 1986 (when the 1972–1973 and 1982–1983 events occurred) (Figure 4d). Thus it is possible that the net impact of an EN event on the CCS will depend greatly on the ambient conditions present at the time of the impact. Other ambient conditions with the potential to modulate the EN impact include a relatively weak thermocline between 1950 and 1969, with a strengthening trend afterward (Figure 4b), and

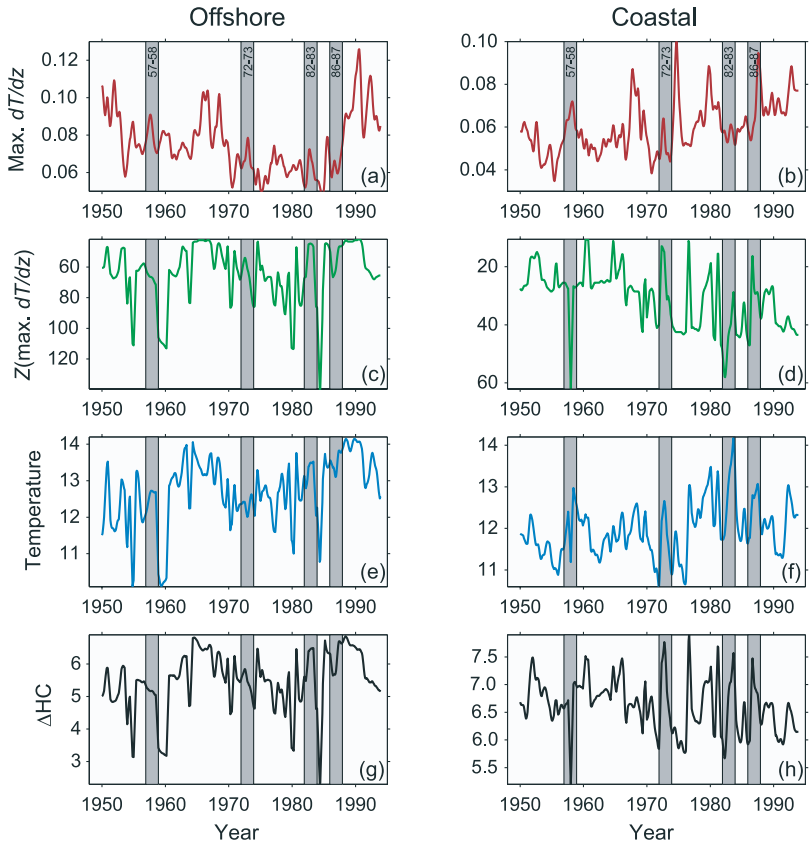

Figure 4. Monthly time series at example locations (left column) 5 and (right column) 6 for (a, b) maximum dT/dz (°C m^{-1}), (c, d) depth of the maximum dT/dz (m), (e, f) temperature at the depth of the maximum dT/dz (°C), and (g, h) heat content difference between the two depths of integration ($\times$ 10^9 J m^{-2}). Four major El Niño events are highlighted by the gray bars.

a cool thermocline between 1950 and 1975, followed by a warm period between 1976 and 1988 (Figure 4f).

3.3. Mean Seasonal Patterns and Seasonal Nonstationarity

[19] Cross-shore and alongshore patterns in strength and depth of the thermocline are evident in the seasonal component (Figures 5 and 6). In general, the strength of the thermocline reaches its annual minimum in February–March and its annual maximum in August–September at the coastal locations, while at the offshore locations the minimum is reached in March–April and the maximum in September–October. The amplitude of the coastal seasonal cycle is large at location 2 and decreases steadily toward the north, while at the offshore locations the amplitude is of similar magnitude among locations (Figure 5).

[20] A shallow permanent thermocline at the coastal locations precludes large annual excursions toward the surface, although there is a slight increase in amplitude from south to north as the permanent thermocline deepens (Figure 6). The coastal thermocline is deepest around January and shallowest around July. Offshore, the greatest deepening occurs in February–March and the greatest shoaling in August–September. This onshore-offshore lag of about 1 month is consistent with westward propagating Rossby waves [e.g., *White*, 1985; *White et al.*, 1990]. Seasonal shoaling is of smaller magnitude and tends to occur earlier in the year as one moves from south to north at the offshore locations (Figure 6).

[21] Except for location 2, which displays mostly stationary seasonal cycles, all other locations feature marked variations in the year-to-year amplitude and phase of the seasonal component (Figures 5 and 6). Amplitude variability in thermocline strength and depth is characterized by periods of about 3–5 years of alternating weakened/enhanced and deeper/shallower seasonal extrema, respectively. Variations in winter minima and summer maxima are generally in the same direction (i.e., the annual amplitude is relatively unchanged from year to year), but there are times when they vary in opposite directions, or when the annual amplitude is primarily driven by only one of the seasonal extrema. At most locations the timing of the minima and maxima are seen to fluctuate by a few months, resulting in seasons of shorter or longer duration (Figures 5 and 6).

[22] The low-frequency behavior of the seasonal component is examined in more detail at offshore location 5 and coastal location 6 (Figure 7). At location 5, the strength of the thermocline underwent a gradual reduction in amplitude from the start of the series until about 1980, driven initially by a decrease in summertime maxima, but also by an increase in wintertime minima after about 1970. The increased amplitude after 1982 was mostly associated with a weakening of wintertime minima (Figure 7a). A long-term

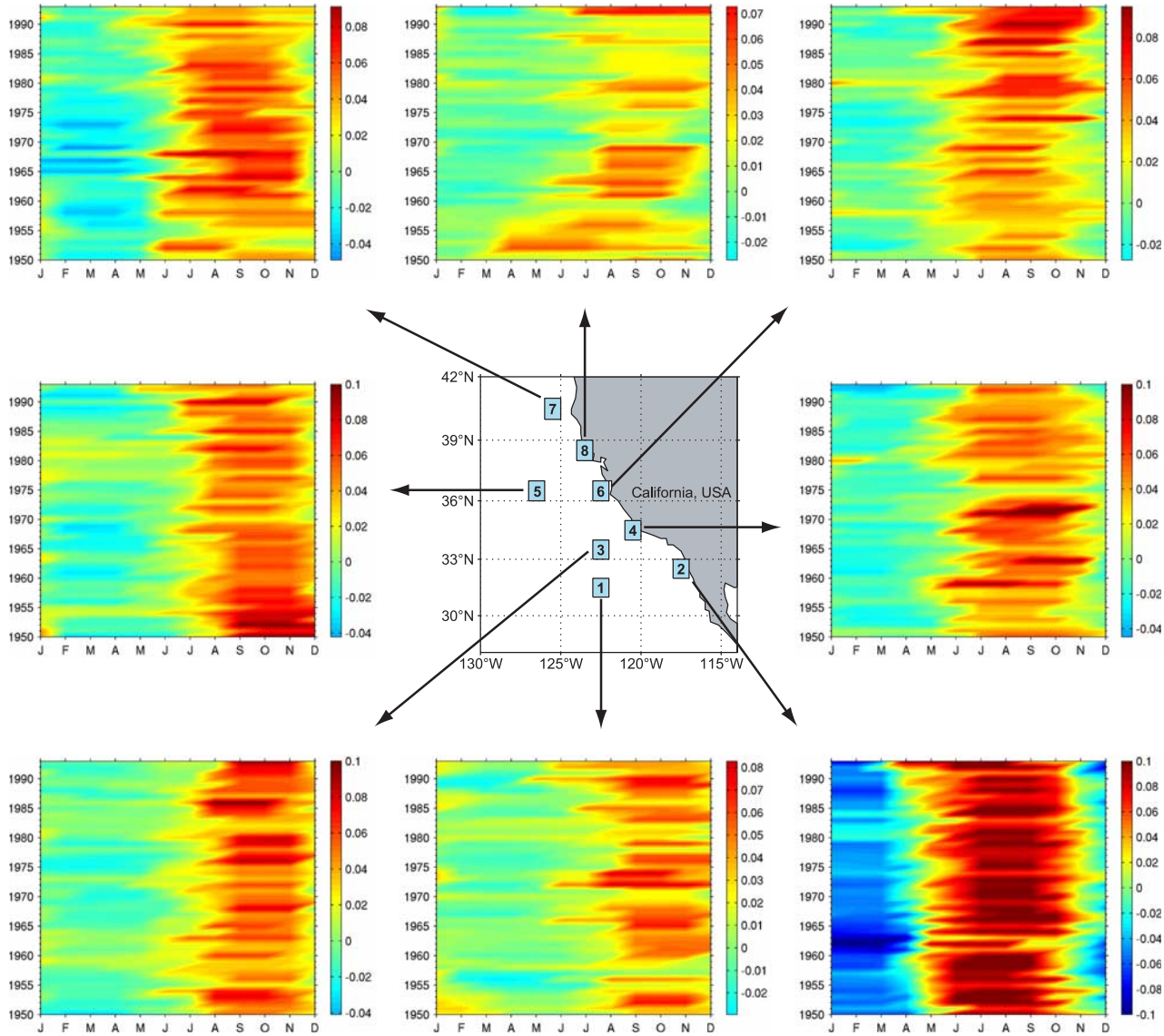

Figure 5. Seasonal component of maximum dT/dz (°C m^{-1}) at eight locations in the CCS, 1950–1993.

shift in the timing of the seasonal maximum is also noted, from November at the start of the series to September at the end (Figure 5). At the coastal location, the low-frequency behavior of the seasonal cycle is punctuated by two periods of increased thermocline strength lasting through the year, one between 1956 and 1961, and the other between 1977 and 1982 (Figure 7b). An increase in the seasonal amplitude is seen between 1983 and the end of the record, resulting from both lowered winter minima and enhanced summer maxima. With regard to thermocline depth, the seasonal amplitude at the offshore location remained relatively constant throughout the record, but the mean level showed a decadal pattern of alternating shoaling and deepening trends, with change points around 1958, 1966, 1979, and 1989 (Figure 7c). Finally, at the coastal location, summertime shoaling remained at a relatively stable level throughout the record, but the wintertime thermocline showed a deepening trend until about 1963 (Figure 7d) that was seen at all coastal locations (not shown). The timing of maximal seasonal deepening also tended to shift from January to December during these periods (Figure 6).

4. Discussion

4.1. Forcing of Long-Term Trends

[23] The common trend analysis of subsurface temperatures of *Mendelssohn et al.* [2003] identified differing tendencies above and within the thermocline over the 1950–1993 period, which they interpreted as evidence for long-term changes in stratification in the CCS. Analysis of variables describing the depth range of maximum stratification in the water column in this study revealed tendencies consistent with a strengthening and deepening of the thermocline at the coast, and a weakening and shoaling offshore. More specifically, between 1950 and 1993, the thermocline strengthened by 30–44% and deepened by 35–82% at the coastal locations, while it weakened by 7–23% and shoaled by 10–17% at the offshore locations.

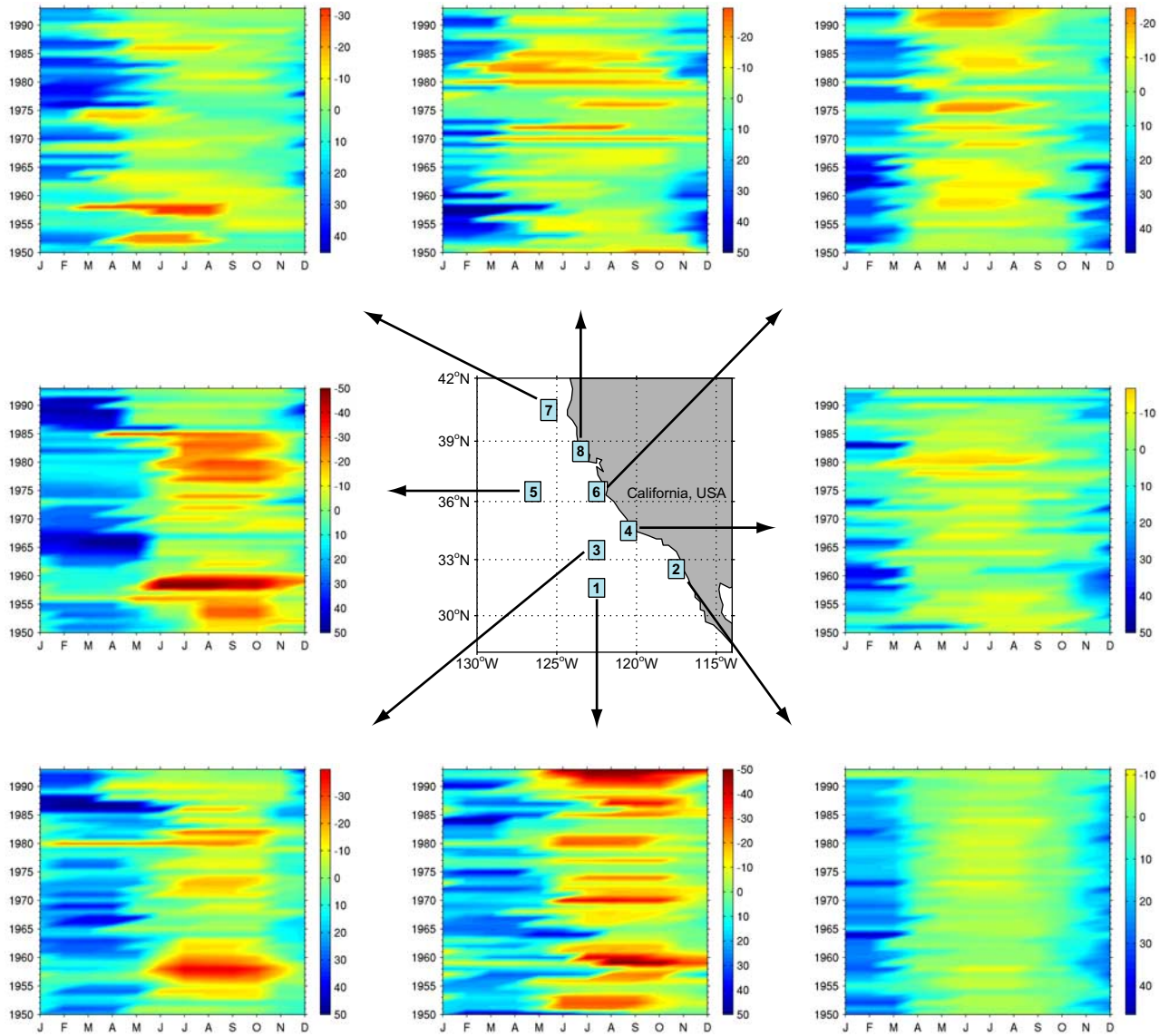

Figure 6. Seasonal component of depth of maximum dT/dz (m) at eight locations in the CCS, 1950–1993. Note that the vertical (depth) scale has been reversed to facilitate interpretation. Negative values (warm colors) indicate displacements of the thermocline toward the surface, while positive values (cool colors) represent deepening.

These changes imply a flattening of the cross-shore slope of the isotherms set up by Ekman divergence at the coast, and suggest a slowing of equatorward geostrophic flow in the portion of the CCS between 40°N and 31°N. A concurrent trend of stronger positive wind stress curl at the coast and a weakening offshore [*Di Lorenzo et al.*, 2004] may be the forcing mechanism for this pattern. This trend in the wind stress curl has been linked to an intensification of the cyclonic circulation of the Southern California Eddy [*Di Lorenzo et al.*, 2004], which may account for the unique weakening and deepening trends of the thermocline at coastal location 2.

[24] Underlying the observed linear tendencies was a substantial decadal variability (Figures 2 and 3). Much of the decadal-scale changes in the CCS are driven by remote forcing, through changes in wind stress in the midlatitudes of the central North Pacific [*Parrish et al.*, 2000]. These regional changes are associated with variations in the intensity of the Aleutian Low pressure system, and the resulting changes in mixed layer depth, sea surface temperature, and current transports manifest themselves in the CCS through basin-wide redistributions of thermal energy and mass, as well as through geostrophic adjustments [*Parrish et al.*, 2000]. Decadal changes in stratification and thermocline depth have specifically been linked to changes in wind stress forcing through a redistribution of energy to the higher-order baroclinic modes, at least in the equatorial Pacific [*Moon et al.*, 2004]. However, local responses to large-scale forcing (e.g., Ekman dynamics) may also play a role in the observed decadal variability in the CCS.

[25] Our analysis further showed that thermocline temperatures and water column heat content have significantly increased at all locations. Heat content gains in the upper 200 m have been on the order of 6.2–9.1% at the coast and

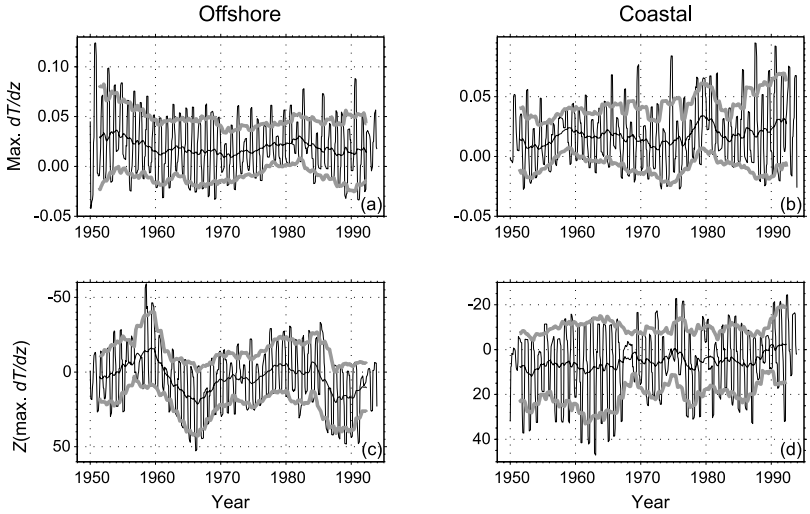

Figure 7. Monthly time series at example locations (left column) 5 and (right column) 6 for seasonal component of (a, b) maximum dT/dz (°C m^{-1}), and (c, d) depth of the maximum dT/dz (m). Smooth black curve is a 37-point running mean, and heavy gray curves are the corresponding ±1 standard deviation envelope around the 37-point sliding window, drawn to enhance low-frequency variability.

2.4–7.1% offshore. These findings are consistent with a low-frequency warming trend of about 1°C over the last 50 years that has been detected in surface and subsurface temperature records throughout the CCS [e.g., *Roemmich*, 1992; *Schwing and Mendelssohn*, 1997; *Mendelssohn et al.*, 2003]. *Di Lorenzo et al.* [2004] have recently linked this warming with a period of mostly positive net surface heat fluxes between 1970 and 1998 over the North Pacific Ocean. However, a net warming signal beginning in the 1970s has been detected throughout the Pacific Ocean, and indeed in all major basins of the world ocean [*Levitus et al.*, 2000], appearing to arise from a combination of natural and anthropogenic sources of radiative forcing on the global climate system [*Levitus et al.*, 2001].

4.2. Forcing of Seasonal Trends

[26] The 1-month lag in the timing of the seasonal extrema at the offshore locations relative to the coastal locations in both strength and depth of the thermocline (Figures 5 and 6) may be related to the westward propagation of seasonal Rossby waves induced by thermocline perturbations [e.g., *White*, 1985; *White et al.*, 1990]. However, since the thermocline is strongly tied to the seasonal cycle of wind stress curl along the coast, it is also possible that the observed lag could be related to a slower ocean response to weaker (or negative) wind stress curl in the offshore region relative to the stronger positive curl near the coast year-round. Wind stress curl also peaks later in the year away from the coast, and its effect on the depth of the thermocline is less clear there [*Murphree et al.*, 2003].

[27] The seasonal trends in thermocline strength and depth consisted of alternating periods of weakened and enhanced annual cycles lasting 3–5 years, although this was highly variable among locations. Some, but not all, of these fluctuations appear to be related to EN events. A few locations also showed a higher amplitude of the seasonal range in the early part of the record, followed by a period of low annual variability in the middle, and then by a return to higher annual variability toward the end (e.g., Figure 7a). This is similar to the common seasonal trends of subsurface temperatures reported by *Mendelssohn et al.* [2004]. Finally, the variability in trends among locations implies that local processes are important in shaping the amplitude and phase of the seasonal thermocline. Therefore the effects of this local variability should be considered when assessing the net effects of the long-term, remotely forced trends described in the previous section.

4.3. Biological Implications

[28] Long-term, low frequency changes involving the region of maximum vertical stratification of the kind presented in this study can have profound ecological impacts through changes in the vertical fluxes of nutrients from below, which in turn support biological production in the surface layers. In the southern part of the CCS, *McGowan et al.* [2003] have documented a 17% deepening in the depth of the 12°C isotherm (a proxy for thermocline depth and nutricline depth) for the period 1976–2000 with respect to 1950–1975. Coincident with this deepening was a 74% decline in zooplankton biomass. These authors also reviewed a compelling body of evidence pointing to dramatic declines in marine populations involving at least four trophic levels and a large number of taxa over the same period [*McGowan et al.*, 2003]. To explain this biological response, *McGowan et al.* [2003] proposed a positive feedback mechanism whereby the observed near-surface warming led to increased stratification, which resulted in reduced input of colder, more saline and more nutrient-rich waters from below, which in turn caused further increases in the stability of the water column. Our results, which generally agree with this scenario, would extend the impact to a much larger region in the CCS.

[29] There is evidence that low-frequency perturbations to the annual cycle can also have biological and ecological repercussions. For instance, *Beare and McKenzie* [1999] have documented a decline in the abundance of the copepod *Calanus finmarchicus* in the North Sea in conjunction with a decrease in the seasonal amplitude and a shift in the phase

of the North Atlantic Oscillation. In the southern CCS, *McGowan et al.* [2003] reported a 2-month shift in the seasonal mean peak in zooplankton biomass, from July during the cold conditions that characterized the period 1950–1975, to May during the subsequent warm period 1976–2000. Thus a stronger summer thermocline or an extended wintertime deepening, if recurring over several years, could potentially alter the optimal conditions for phenological functions such as the timing of the phytoplankton bloom, fish spawning, duration of larval stages, etc. It is clear that more long-term observations are needed to better understand how ocean ecosystems respond to these types of climatic variations.

5. Summary and Conclusions

[30] State-space models have allowed us to detect and characterize changes in thermal stratification in the CCS over the period 1950–1993 at multiple timescales. We have focused on the low-frequency behavior of the long-term mean level and the seasonal cycle. The main findings of the study can be summarized as follows:

[31] 1. Between 1950 and 1993, the mean level of the coastal thermocline strengthened and deepened, while it weakened and shoaled offshore. Water column heat content and the temperature of the thermocline significantly increased throughout the study area.

[32] 2. Substantial decadal variability superimposed on these linear tendencies may play a role in determining the magnitude of the response of the upper ocean to interannual events such as El Niño. This may explain the different response to the 1957–1958 event, when the thermocline was shallow, and those of subsequent events that took place during a period when the thermocline was depressed.

[33] 3. The seasonal component of thermocline depth and strength was highly nonstationary. Alternating periods of weakened and enhanced annual cycles lasting 3–5 years characterized these series, although the patterns were not very coherent among locations. These results demonstrate the importance of independent assessment of seasonal variability in a time series and its interaction with long-term climatic trends.

[34] 4. The Southern California Bight, represented in this study by location 2, featured a shallow, warm thermocline with weakening and deepening tendencies. In addition, this was the only location where the seasonal component was nearly stationary. The unique behavior at this coastal location suggests a greater influence of water from a different (probably southern) source than the rest of the CCS. It may also be related to local forcing associated with the recirculation of the Southern California Eddy.

[35] The low-frequency response of the thermocline appears to be coupled with well-documented trends in large-scale atmospheric forcing, although variability imparted by local gradients may also play a role, particularly at the seasonal scale. Ultimately, however, the in situ process of diminished vertical fluxes of nutrients to the upper layers in response to long-term warming and enhanced stratification is probably the cause for the deterioration of the productive ecosystems of the CCS [cf. *McGowan et al.*, 2003].

[36] *Schwing and Mendelssohn* [1997] have demonstrated that along with the long-term warming tendency in sea surface temperatures in the CCS, there has been a systematic, but much smaller cooling tendency driven by enhanced spring-summer upwelling-favorable wind stress along the coast. These results reveal the complex nature and interactions of different processes at work in the CCS, and illustrate the need for a better understanding of the upwelling process in the context of ambient conditions and their ecological effects. For instance, the standard coastal upwelling index [e.g., *Schwing et al.*, 1996], although widely used in marine ecosystem studies, simply provides an estimate of surface Ekman transport, but does not contain information on the biological utility of the upwelling process. We have developed and are currently testing a new Biologically Effective Upwelling and Transport Index (BEUTI), which incorporates water column information like the degree of stratification and the nutrient content of the upwelled water (D. Palacios et al., manuscript in preparation, 2004).

[37] Finally, a climate shift, from a warm, low-production regime to a cool, highly productive regime, appears to have occurred in the CCS after 1998 [*Schwing and Moore*, 2000; *Schwing et al.*, 2000]. It is presumed that an intensification of the North Pacific High pressure system has led to anomalously strong coastal upwelling-favorable winds and greater than normal southward transport, favoring the rebound of cold water zooplankton and fish populations in the CCS [*Peterson and Schwing*, 2003]. If sustained, these conditions could lead to long-term trends in the coastal thermocline opposite to those reported here (i.e., weakening, shoaling), and to ecosystem-wide changes in structure and production.

[38] **Acknowledgments.** We thank Lynn deWitt for her initial work on the data set. This work was performed while the first author held a National Research Council Research Associateship Award at the Pacific Fisheries Environmental Laboratory. Support came from a grant from the U.S. GLOBEC Northeast Pacific Program, and from the NOAA Fisheries and the Environment Program. The manuscript benefited from comments by A. W. Leising, R. H. Parrish, A. J. Miller, and two anonymous reviewers. This is U.S. GLOBEC contribution 486.

References

Beare, D. J., and E. McKenzie (1999), Connecting ecological and physical time-series: The potential role of changing seasonality, *Mar. Ecol. Prog. Ser.*, *178*, 307–309.

Beare, D. J., E. McKenzie, and D. C. Speirs (1998), The unstable seasonality of *Calanus finmarchicus* in the Fair Isle Current, *J. Mar. Biol. Assoc. U.K.*, *78*, 1377–1380.

Bograd, S. J., F. B. Schwing, R. Mendelssohn, and P. Green-Jessen (2002), On the changing seasonality over the North Pacific, *Geophys. Res. Lett.*, *29*(4), 1333, doi:10.1029/2001GL013790.

Broekhuizen, N., and E. McKenzie (1995), Patterns of abundance for *Calanus* and smaller copepods in the North Sea: Time series decomposition of two CPR data sets, *Mar. Ecol. Prog. Ser.*, *118*, 103–120.

Chelton, D. B., P. A. Bernal, and J. A. McGowan (1982), Large-scale interannual physical and biological interaction in the California Current, *J. Mar. Res.*, *40*, 1095–1125.

Conkright, M. E., et al. (1999), World Ocean Database 1998, documentation and quality control, version 2.0, *Internal Rep. 14*, Ocean Clim. Lab., Natl. Oceanic and Atmos. Admin., Silver Spring, Md.

Cushing, D. H. (1969), The regularity of the spawning season of some fishes, *J. Cons. Cons. Int. Explor. Mer.*, *33*, 81–92.

Cushing, D. H. (1975), *Marine Ecology and Fisheries*, 277 pp., Cambridge Univ. Press, New York.

Di Lorenzo, E., A. J. Miller, N. Schneider, and J. C. McWilliams (2004), The warming of the California Current: Dynamics and ecosystem implications, *J. Phys. Oceanogr.*, in press.

Durand, M.-H., and R. Mendelssohn (1998), How to detect a change both on global and local scale in oceanographic time series, in *Global Versus Local Changes in Upwelling Systems*, edited by M.-H. Durand et al., pp. 45–78, Ed. de L'Orstom, Paris.

Field, D. B. (2004), Variability in vertical distributions of planktonic foraminifera in the California Current: Relationships to vertical ocean structure, *Paleoceanography*, *19*, PA2014, doi:10.1029/2003PA000970.

Kara, A. B., P. A. Rochford, and H. E. Hurlburt (2003), Mixed layer depth variability over the global ocean, *J. Geophys. Res.*, *108*(C3), 3079, doi:10.1029/2000JC000736.

Le Quéré, C., O. Aumont, P. Monfray, and J. Orr (2003), Propagation of climatic events on ocean stratification, marine biology, and CO_2: Case studies over the 1979–1999 period, *J. Geophys. Res.*, *108*(C12), 3375, doi:10.1029/2001JC000920.

Levitus, S., J. I. Antonov, T. P. Boyer, and C. Stephens (2000), Warming of the world ocean, *Science*, *287*, 2225–2229.

Levitus, S., J. I. Antonov, J. Wang, T. L. Delworth, K. W. Dixon, and A. J. Broccoli (2001), Anthropogenic warming of the Earth's climate system, *Science*, *292*, 267–270.

Lynn, R. J., S. J. Bograd, T. K. Chereskin, and A. Huyer (2003), Seasonal renewal of the California Current: The spring transition off California, *J. Geophys. Res.*, *108*(C8), 3279, doi:10.1029/2003JC001787.

McGowan, J. A., S. J. Bograd, R. J. Lynn, and A. J. Miller (2003), The biological response to the 1977 regime shift in the California Current, *Deep Sea Res., Part II*, *50*(14–16), 2567–2582.

Mendelssohn, R., F. B. Schwing, and S. J. Bograd (2003), Spatial structure of subsurface temperature variability in the California Current, 1950–1993, *J. Geophys. Res.*, *108*(C3), 3039, doi:10.1029/2002JC001568.

Mendelssohn, R., F. B. Schwing, and S. J. Bograd (2004), Nonstationary seasonality of upper-ocean temperature in the California Current, *J. Geophys. Res.*, doi:10.1029/2004JC002330, in press.

Moon, B.-K., S.-W. Yeh, B. Dewitte, J.-G. Jhun, I.-S. Kang, and B. P. Kirtman (2004), Vertical structure variability in the equatorial Pacific before and after the Pacific climate shift of the 1970s, *Geophys. Res. Lett.*, *31*, L03203, doi:10.1029/2003GL018829.

Murphree, T., P. Green-Jessen, F. B. Schwing, and S. J. Bograd (2003), The seasonal cycle of wind stress curl and its relationship to subsurface ocean temperature in the Northeast Pacific, *Geophys. Res. Lett.*, *30*(9), 1469, doi:10.1029/2002GL016366.

Parrish, R. H., F. B. Schwing, and R. Mendelssohn (2000), Mid-latitude wind stress: The energy source for climatic shifts in the North Pacific Ocean, *Fish. Oceanogr.*, *9*, 224–238.

Peterson, W. T., and F. B. Schwing (2003), A new climate regime in northeast Pacific ecosystems, *Geophys. Res. Lett.*, *30*(17), 1896, doi:10.1029/2003GL017528.

Roemmich, D. (1992), Ocean warming and sea-level rise along the southwest United States coast, *Science*, *257*, 373–375.

Roemmich, D., and J. A. McGowan (1995), Climatic warming and the decline of zooplankton in the California Current, *Science*, *267*, 1324–1326.

Schwing, F. B., and R. Mendelssohn (1997), Increased coastal upwelling in the California Current System, *J. Geophys. Res.*, *102*, 3421–3438.

Schwing, F. B., and R. Mendelssohn (1998), Long-term variability in the seasonality of Eastern Boundary Current (EBC) Systems: An example of increased upwelling from the California Current, in *Global Versus Local Changes in Upwelling Systems*, edited by M.-H. Durand et al., pp. 79–100, Ed. de L'Orstom, Paris.

Schwing, F. B., and C. S. Moore (2000), A year without summer for California, or a harbinger of a climate shift?, *Eos Trans. AGU*, *81*(27), 304–305.

Schwing, F. B., M. O'Farrell, J. M. Steger, and K. Baltz (1996), Coastal upwelling indices, west coast of North America, 1946–95, *NOAA Tech. Memo. NOAA-TM-NMFS-SWFSC-231*, 144 pp., Natl. Oceanic and Atmos. Admin., Natl. Mar. Fish. Serv., La Jolla, Calif.

Schwing, F., C. Moore, S. Ralston, and K. A. Sakuma (2000), Record coastal upwelling in the California Current in 1999, *Calif. Coop. Oceanic Fish. Invest. Rep.*, *41*, 148–160.

White, W. B. (1985), The resonant response of interannual baroclinic Rossby waves to wind forcing in the eastern mid-latitude North Pacific, *J. Phys. Oceanogr.*, *15*, 403–415.

White, W. B., C.-K. Tai, and J. DiMento (1990), Annual Rossby wave characteristics in the California Current region from the GEOSAT exact repeat mission, *J. Phys Oceanogr.*, *20*, 1297–1311.

S. J. Bograd, R. Mendelssohn, D. M. Palacios, and F. B. Schwing, Pacific Fisheries Environmental Laboratory, National Marine Fisheries Service, NOAA, 1352 Lighthouse Avenue, Pacific Grove, CA 93950-2097, USA. (dpalacios@pfeg.noaa.gov)